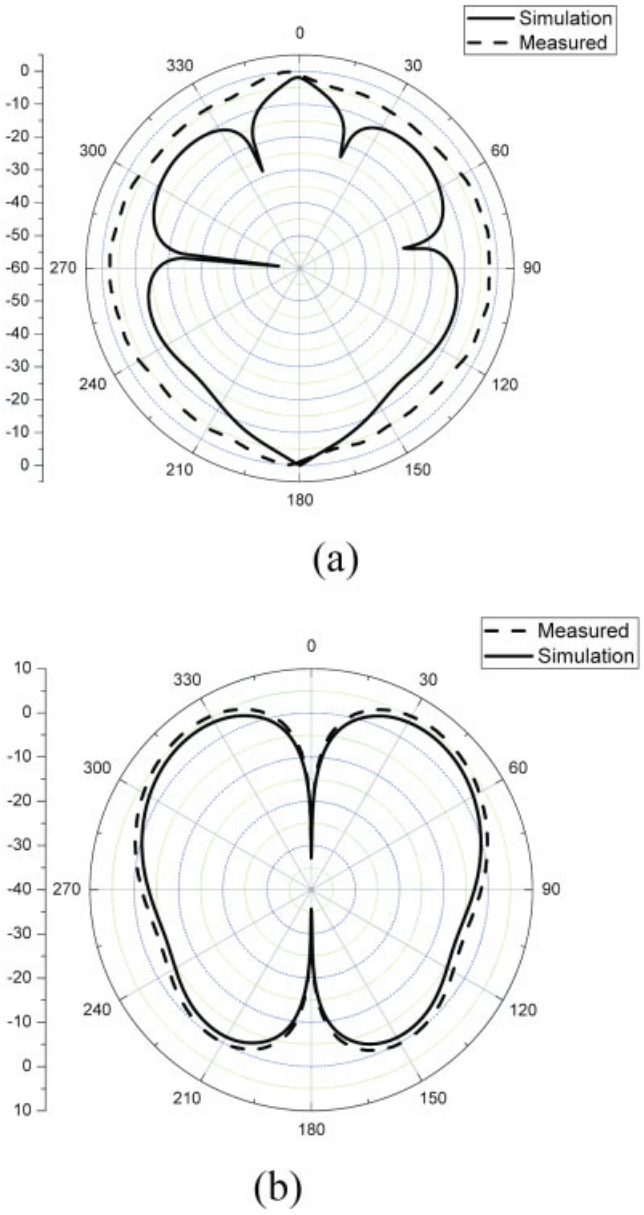

Figure 8 Simulated and measured radiation patterns for capacitance coupled antenna with vertical-slot walls. (a) *E*-plane, (b) *H*-plane. [Color figure can be viewed in the online issue, which is available at www.interscience.wiley.com]

radiation pattern across the operating frequency band and we can regard it as a monopole radiating patch antenna.

4. CONCLUSIONS

The capacitive coupled antenna with additional radiation element is discussed in this letter, this antenna has butterfly-like radiation pattern. Four metal strips are connected between the radiation element and the ground to reduce the size of the antenna. One vertical-slot wall is added on the circular ground to enhance the bandwidth of the antenna. Both the simulations and experiments indicate more than 60% bandwidth improvement over the antenna without vertical-slot walls. The measured gain of the antenna with vertical-slot wall is about 6 dB.

ACKNOWLEDGMENTS

The authors would like to express their gratitude to the financial support of the National Science Foundation of China under Grant 60471025; sincere thanks also goes to Ms. Ziying Liu for her Laboratory assistance.

REFERENCES

1. A.K. Shackelford, K.F. Lee, K.M. Luk, and R.C. Chair, U-slot patch antenna with shorting pin, Electron Lett 37 (2001), 729–730.
2. Y.X. Guo, C.L. Mak, K.M. Luk, and K.F. Lee, Analysis and design of L-probe proximity fed-patch antennas, IEEE Trans Antenn Propag 49 (2001), 145–149.
3. J.-H. Jung, H. Choo, Y. Moon, Y.-E. Kim, and I. Park, Electromagnetic coupled fed disk-loaded monopole antenna with multiple shorting pins, IEEE Int Workshop Antenna Technol 37 (2005), 242–245.
4. N.P. Agrawall, G. Kumar, and K.P. Ray, Wide-band planar monopole antennas, IEEE Trans Antenn Propag AP-46 (1998), 294–295.
5. L. Economou and R.J. Langley, Patch antenna equivalent to simple monopole, Electron Lett 33 (1997), 121–729.
6. H. Nakano and Tokyo, A meander spiral antenna, Antenn Propag Soc Int Symp 3 (2004), 2243–2246.
7. Z. Qi and C. Chang, Analysis of micro-strip antennas loaded with shorting-pin, Antenn Propag Soc Int Symp A 3, Washington, DC (2005), 138–141.

SELFHOMODYNE PHOTONIC MICROWAVE RECEIVER ARCHITECTURE BASED ON LINEAR OPTICAL MODULATION AND FILTERING

Mani Hossein-Zadeh[1] and A. F. J. Levi[2]

[1] Department of Applied Physics, California Institute of Technology, CA

[2] Department of Electrical Engineering, University of Southern California, CA; Corresponding author: mhz@caltech.edu

Received 25 June 2007

ABSTRACT: *We present a self-homodyne photonic microwave receiver architecture that uses linear optical modulation and optical filtering for data down-conversion from a microwave carrier. Preliminary results demonstrate the feasibility of this technique for demodulating up to 100 Mb/s digital data from carrier frequencies above 10 GHz.* © 2007 Wiley Periodicals, Inc. Microwave Opt Technol Lett 50: 345–350, 2008; Published online in Wiley InterScience (www.interscience.wiley.com). DOI 10.1002/mop.23065

Key words: *RF-photonics; RF down-conversion; self-homodyne receiver*

1. INTRODUCTION

RF-photonics is a promising technology for many RF and millimeter wave applications such as wireless LAN, CATV, phased array antenna radar, and cellular communications [1–5]. Up-conversion to optical frequencies provides extended bandwidth for data communication that reduces the transmission loss in high-frequency RF links and enables electromagnetic isolation from the environment. Moreover RF-to-optical conversion enables photonic processing of RF signals that can reduce the complexity of front-end RF hardware in wireless communication systems.

Here we present a technique for data down-conversion from a transmitted carrier RF signal in the optical domain. In our pro-

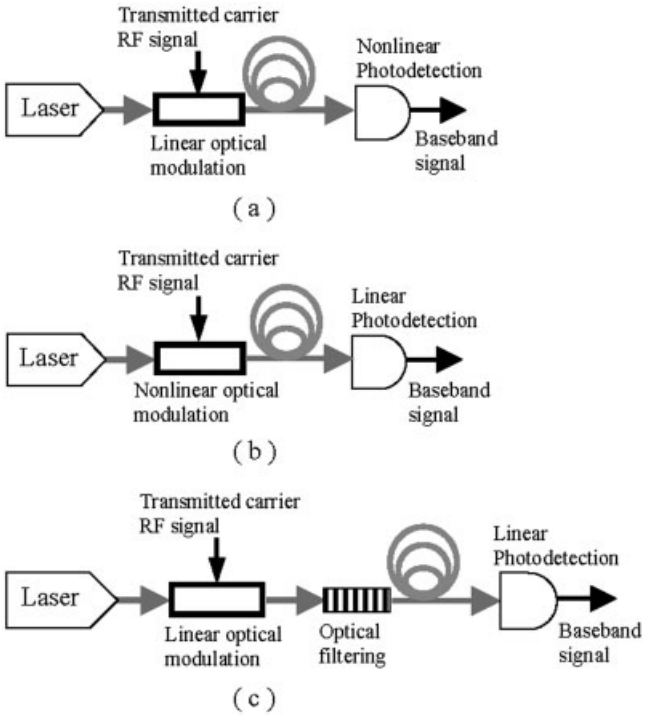

Figure 1 Three possible architectures for photonic down-conversion in a selfhomodyne RF receiver. (a) Nonlinear photodetection [7]. (b) Nonlinear optical modulation [8]. (c) Postmodulation optical filtering (current work)

posed architecture, modifying the optical spectrum of a linearly modulated optical carrier results in direct generation of baseband modulated photocurrent upon detection. This technique may be used to eliminate the post detection RF-down-conversion stage in radio-over-fiber wireless access systems.

2. PHOTONIC SELFHOMODYNE RECEIVER

In a direct conversion or homodyne RF receiver, baseband information is obtained by mixing the received signal and the local oscillator (LO) with zero intermediate frequency (IF) [6]. If enough transmitted carrier RF power is received it is possible to eliminate the LO and mix the RF carrier and the sidebands in a nonlinear device (self-mixer) to down-convert the information from the received signal. Because the received signal is mixed with itself and the IF is zero, it is referred to as self-homodyne detection. In short distance high-frequency wireless links the relatively low power-efficiency of the self-homodyne down-conversion technique may be justified because of reduced complexity and low-power consumption in the receiver.

The concept of self-homodyne down-conversion from a transmitted carrier RF signal can be used to design a photonic RF receiver where electronic self-mixing is replaced by photonic self-mixing in the optical domain. In this case the received RF signal is up-converted to optical frequencies and, after photonic signal processing a baseband-modulated photocurrent can be generated upon detection.

Figure 1 shows three possible receiver architectures for self-homodyne down-conversion in the optical domain. In the first design [Fig. 1(a)] the RF signal modulates the optical carrier in a linear electro-optic (EO) modulator. After transmission through the optical link a nonlinear photodetector simultaneously down-converts the baseband and generates the corresponding photocurrent [7]. In the second design [Fig. 1(b)] nonlinear EO modulation of the optical carrier by the RF signal generates a baseband modulated optical carrier. After transmission a linear photodetector can generate the baseband current [8, 9]. In these designs self-mixing is realized using the nonliearity in either the modulation or detection process. However, conventional modulators and photodetectors are designed for linear response consequently their nonlinear operation requires special design and is usually inefficient. Here we propose a third approach that uses conventional photonic devices that are optimized for linear operation. As shown in Figure 1(c), in this design the RF signal modulates the optical carrier in a linear EO modulator. Subsequently the spectrum of the modulated optical carrier is modified using an optical filter such that linear detection of electromagnetic intensity generates the baseband photocurrent.

3. RF DOWN-CONVERSION USING LINEAR OPTICAL MODULATION AND OPTICAL FILTERING

In this section we show that tailoring the optical output spectrum of a linear EO modulator driven by an RF signal (baseband modulated RF carrier) can generate a baseband-modulated photocurrent upon linear photodetection. For simplicity let us assume that the RF carrier is modulated by a pure sinusoidal baseband so that the voltage of the received RF signal can be written as:

$$V_{RF}(t) = V_0(1 + m\cos(\omega_b t))\cos(\omega_{RF} t) \quad (1)$$

where ω_b is the baseband frequency, ω_{RF} is the RF carrier frequency, m is the RF modulation index, and V_0 is amplitude of the RF voltage. Linear EO amplitude modulation of an optical carrier (ω_{opt}) by V_{RF} generates an optical field (E_{opt}) with the following form:

$$E_{opt}(t) = E_0[1 + M(1 + m\cos(\omega_b t))\cos(\omega_{RF} t)]\cos(\omega_{opt} t) \quad (2)$$

where E_0 is the amplitude of the optical carrier and M is the optical modulation index. Note that $\omega_{opt} = 2\pi f_{opt}$ is in the $f_{opt} = 200$ THz frequency regime while ω_b and ω_{RF} are typically in the MHz and GHz frequency regimes, respectively. Figure 2 shows the frequency spectrum of the optical signal expressed by Eq. (2). In the frequency domain amplitude modulation of the optical wave generates two sidebands around the optical carrier where each sideband consists of a baseband modulated RF carrier. Basically these sidebands are RF signals up-converted to optical frequencies hence we refer to them as "RF-optical" sidebands.

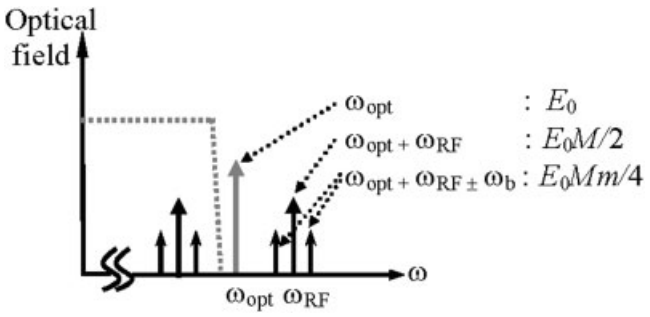

Figure 2 Schematic diagram of the frequency spectrum of an optical-carrier (ω_{opt}) modulated by an RF signal. The RF signal is an RF-carrier modulated by a single-tone baseband signal (with a transmitted carrier modulation format). The amplitude of each frequency component is written as a function of the optical-field (E_0) and the RF and optical modulation indexes (m and M, respectively)

The amplitude of each frequency component is determined by the RF and optical modulation indices (m and M respectively) as well as the amplitude of the optical carrier (E_0). Evidently the intensity of the optical signal expressed by Eq. (2) generates a photocurrent proportional to V_{RF} [Eq. (1)]. However if the optical carrier and the upper RF-optical sideband are rejected using a low-pass optical filter (dashed line in Fig. 2), the modified optical field (E_0') and transmitted optical power (P_{opt}) can be written as:

$$E_{opt}'(t) = \mathrm{Re}\frac{ME_0}{2}\left[\frac{m}{2}(e^{i(\omega_{opt}-\omega_{RF}-\omega_b)} + e^{i(\omega_{opt}-\omega_{RF}+\omega_b)}) + e^{i(\omega_{opt}-\omega_{RF})}\right] \tag{3}$$

$$\mathbf{P}_{opt}(\mathbf{t}) \propto |\mathbf{E}'_{opt}(\mathbf{t})|^2 = \frac{\mathbf{M}^2\mathbf{E}_0^2}{4}\left[1 + \frac{\mathbf{m}^2}{2} + 2\mathbf{m}\cos(\omega_b \mathbf{t}) + \frac{\mathbf{m}^2}{2}\cos(2\boldsymbol{\omega}_b \mathbf{t})\right] \tag{4}$$

The spectrum of the transmitted optical power consists of a DC component, the baseband frequency and its second-harmonic. Equation 4 shows that linear photodetection of the modified optical signal [Eq. (3)] is effectively demodulating the baseband signal from the RF carrier. Clearly an efficient down-conversion requires large optical modulation index M as well as large optical input power (E_0^2). The RF modulation index (m) controls the distribution of the optical power among the DC, baseband, and its second-harmonic. Using Eq. (4) the fractional modulated optical power at ω_b and $2\omega_b$ can be written as:

$$\frac{P_{\omega_b}}{P_{tot}} = \frac{2m}{1 + m^2 + 2m} \tag{5}$$

$$\frac{P_{2\omega_b}}{P_{tot}} = \frac{m^2}{2 + 2m^2 + 4m} \tag{6}$$

The linearity of the demodulation can be quantified as the ratio $P_{\omega b}/P_{2\omega b} = 4/m$. A simple analysis based on these relations show that simultaneous optimization of efficiency and linearity imposes a condition on RF modulation index such that $0.5 < m < 0.8$. Note that $m < 2$ corresponds to a transmitted carrier RF modulation format in agreement with the fact that in the absence of a LO the RF signal has to carry enough energy at the carrier frequency to enable the selfhomodyne process. Using the above technique, baseband information can be demodulated from the RF signal by means of linear optical modulation, optical filtering, and linear detection of the optical intensity. Also the bandwidth of the photodetector is determined by the bandwidth of the baseband signal and not the RF carrier so no high-speed electronic component is required for down-conversion from a high-frequency carrier.

4. EXPERIMENTAL RESULTS

Figure 3 shows a schematic diagram of the experimental arrangement used for demonstrating optical demodulation of an RF signal using optical filtering. The RF carrier is modulated by the baseband using an RF mixer. A DC voltage applied to the IF port of a double-balanced mixer controls the RF modulation index (m). The RF signal is fed into an EO modulator and modulates the optical carrier generated by a tunable laser ($f_{opt} = \omega_{opt}/2\pi = 194$ THz). Subsequently the modulated optical carrier passes through a fiber-Bragg-grating (FBG) filter that rejects the optical carrier and the upper RF-optical sideband. Finally, the modified optical signal is

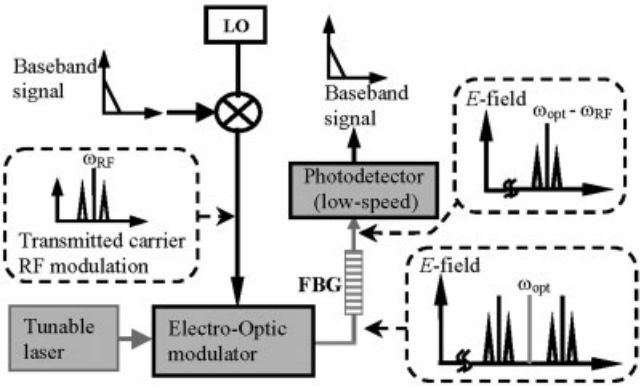

Figure 3 Experimental arrangement for demonstrating photonic RF down-conversion using linear modulation and filtering in optical domain. The diagrams inside the dashed boxes show the frequency spectrum of the signal at different stages

detected in a photodetector that directly generates the baseband current. Qualitatively the down-conversion process can be explained by the fact that the photodiode is a square-law detector for the optical-field (the output current is proportional to the intensity of the optical wave). In the absence of filtering, the photodiode is effectively mixing the optical-carrier (ω_{opt}) with the RF-optical sidebands and generates a photocurrent proportional to original RF signal. When the optical-carrier and one of the RF-optical sidebands are filtered out, the transmitted optical wave is a baseband modulated optical carrier (with a frequency of $\omega_{opt} - \omega_{RF}$) that generates a baseband modulated photocurrent upon linear optical intensity photodetection. The required rejection bandwidth (BW) and role-off slope for efficient rejection (40 dB) of the optical carrier and one of the RF-optical sidebands can be estimated as:

$$\mathbf{BW} > \mathbf{f}_{RF} + \boldsymbol{\Delta}\mathbf{f}_b \tag{7-a}$$

$$\mathbf{Slope}(\mathrm{dB/pm}) > \frac{0.012}{\boldsymbol{\lambda}^2(\mathbf{f}_{RF} - \boldsymbol{\Delta}\mathbf{f}_b)}(\mathrm{dB}) \tag{7-b}$$

where γ_0 is the wavelength of the optical carrier and c is the speed of light. Applying Eq. (7) with $\gamma_0 = 1550$ nm, $f_{RF} = 10$ GHz, and $\Delta f_b = 100$ MHz (a suitable bandwidth for 100 Mb/s data transmission) suggests a BW > 10.1 GHz and Slope > 0.5 dB/pm is needed. The optical filter used in our experiments is a custom made FBG filter with transmission characteristics shown in Figure 4(a). The filter has a very fast role-off of about 1 dB/pm around $\lambda = 1553.15$ nm. The laser source is a tunable single mode device with a linewidth of 0.5 MHz. The electrooptic modulator is a Mach-Zehnder (MZ) modulator with a V_π of 4.5 V and optical insertion loss of 4.5 dB. The output of the photodetector is analyzed with an RF spectrum analyzer.

In the first experiment a 7.6 GHz RF carrier is modulated with a 300 MHz single frequency baseband. Figure 4(b) shows the measured photocurrent spectrum at two different laser wavelengths. By tuning the laser wavelength well above the rejected band ($\lambda_0 = 1553.60$ nm) where the optical carrier and both RF-optical sidebands are transmitted, the spectrum of the photocurrent is simply the spectrum of an amplitude modulated optical wave (the gray line). When the laser wavelength is tuned to the edge of the FBG filter ($\lambda_0 = 1553.28$ nm), where only the lower RF-optical sideband is transmitted, the photocurrent is baseband modulated (the solid black line). The relative alignment of the

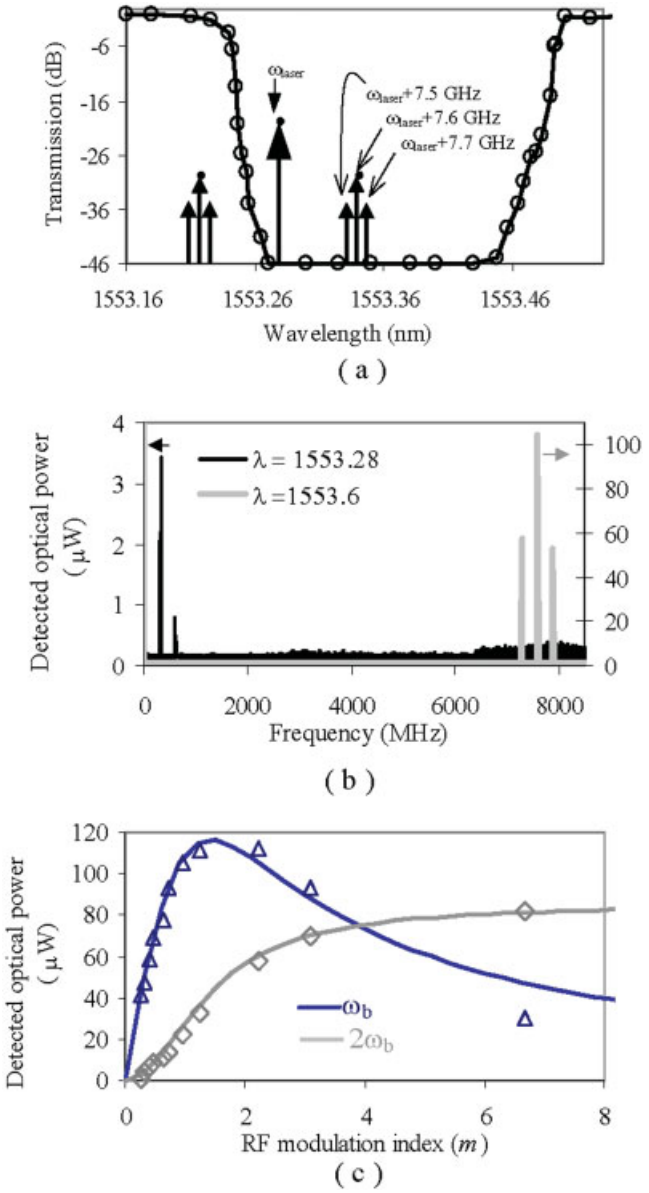

Figure 4 (a) The measured transmission spectrum of the FBG filter. The arrows show the alignment of the spectral components of the modulated optical carrier with respect to the filter response when $\lambda_0 = 1553.28$ nm. (b) The measured spectrum of the detected signal at two different wavelengths (in both cases $m = 0.8$). (c) The magnitude of the detected baseband signal (black triangles) and its second-harmonic (gray diamonds) plotted against RF modulation index (m). The solid lines are the theoretical prediction using Eq. (4). [Color figure can be viewed in the online issue, which is available at www.interscience.wiley.com]

spectral components of the modulated optical carrier with respect to the filter response for this case is shown in Figure 4(a).

To study the effect of the RF modulation index (m) on down-conversion efficiency and linearity of down-conversion, we have measured the magnitude of the down-converted signal and its second-harmonic as a function of m. Figure 4(c) shows the measured optical power at baseband frequency and its second-harmonic plotted against m. The solid lines are theoretical predictions using Eq. (4).

To evaluate the performance of this photonic down-conversion technique we replaced the 300 MHz single-tone with a 10 Mb/s NRZ 2^7-1 PRBS data stream and the wideband photodetector with a digital photoreceiver which had a sensitivity of −41 dBm and a bandwidth of 100 Mb/s. The open triangles in Figure 5(a) are the measured bit error ratio (BER) of the down-converted data plotted against the RF input power.

We repeated the same experiment using a 14.6 GHz $LiNbO_3$ microdisk modulator [8]. The microdisk modulator has a V_{HMM} (half-maximum-modulation voltage [8]) of about 0.6 V and an optical insertion loss of about 10 dB. The laser wavelength is biased for optimized linear modulation. Figure 5(b) shows a photograph of the microdisk modulator. The baseband signal is again a 10 Mb/s NRZ 2^7-1 PRBS bit stream while the carrier frequency is 14.6 GHz. The solid triangles in Figure 5(a) are the measured BER when the MZ modulator is replaced with the microdisk modulator. Because of high resonant microdisk modulator efficiency the sensitivity of receiver is significantly improved even though the RF carrier frequency is double that used for the MZ modulator experiment. Figure 6 shows the measured eye-diagrams (10 and 100 Mb/s) at −18-dBm received RF power for the microdisk-based link

Note that here we are using the microdisk modulator in the linear operating regime as opposed to a previous demonstration of a self-homodyne photonic receiver [8] where nonlinear optical modulation was used [Fig. 1(b)].

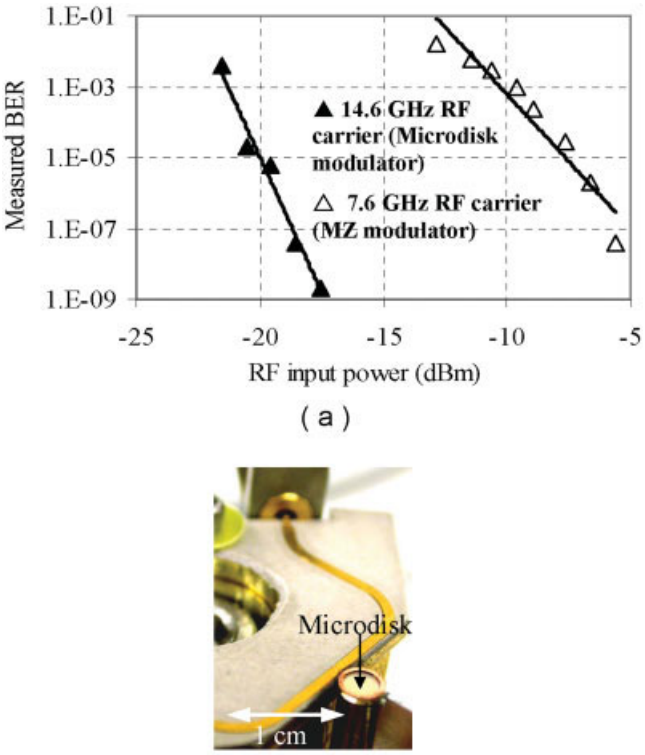

Figure 5 (a) Measured BER of the down-converted data against received RF power for a selfhomodyne photonic RF receiver that employs predetection optical filtering. White triangles: using a MZ modulator with a bandwidth of 10 GHz and a V_π of 4.5 Volt. Black triangles: using a $LiNbO_3$ microdisk modulator with an FSR of 14.6 GHz and a V_{HMM} of 0.6 Volt [8]. The transmitted data for both cases is 10 Mb/S NRZ 2^7-1 PRBS. (b) A photograph of the $LiNbO_3$ microdisk modulator (the microdisk has a diameter of 3 mm and a thickness of 0.4 mm). [Color figure can be viewed in the online issue, which is available at www.interscience.wiley.com]

5. DISCUSSION AND FUTURE PROSPECTS

The photonic self-homodyne RF receiver presented in this work has been demonstrated using discrete photonic devices while in real applications an integrated version is desired. The laser, the microdisk modulator and the detector are relatively small (<1 cm) and in principle can be integrated on a hybrid chip. However, the FBG filter is relatively large (the component used in this work is 7 cm long). An alternative compact optical filter is a high-order microring resonator filter [10] that may be fabricated monolithically in an area less than 1 mm^2. Figure 7(a) shows a schematic diagram of an integrated photonic selfhomodyne RF receiver based on a bandpass multiring filter. The bandpass filter only couples one of the RF-optical sidebands to the drop port so the required bandwidth is $2\Delta f_b$ (as opposed to $f_{RF} + \Delta f_b$ for the notch filter case).

The efficiency of the proposed photonic RF down-conversion technique is relatively low because a large fraction of the optical energy is filtered out and hence does not contribute to the down-conversion process (as opposed to conventional intensity detection where all the spectral components contribute to the photodetection process). Reducing the transmitted optical power of one of the RF-optical sidebands can improve the power efficiency of this passive down-conversion process by a factor of about 1.4 (depending on the value of M and m). This may be achieved using single side-band optical modulation as opposed to the regular amplitude modulation (double side-band) [11, 12]. The single side-band modulation not only improves the power efficiency but also relaxes the required specification for the optical filter. In the absence of one of the RF-optical sidebands the optical filter should only reject the optical carrier, therefore, a single-pole microring with a bandwidth of less than $0.25 \times f_{RF}$ would be sufficient. Figure 7(b) shows the architecture of a photonic self-homodyne RF receiver that employs single-side band modulation and a high-Q microring band-reject filter. One may also consider suppressed carrier optical modulation as an alternative approach that completely eliminates the optical filter. Although suppressed carrier optical modulation has been demonstrated using a MZ modulator [12], the complexity of this scheme compared with optical filtering should be evaluated.

6. CONCLUSION

We have demonstrated a photonic RF receiver architecture that can down-convert baseband information from a transmitted carrier signal by means of linear optical modulation and optical filtering. The system consists of three elements: modulator, filter, and detector. The maximum carrier frequency is determined by the bandwidth of the EO modulator and the maximum data rate is limited by the bandwidth of the photodetector. Therefore the maximum speed of the electronic elements in the receiver is limited by the baseband signal and not the carrier frequency. This architecture may reduce the cost and complexity of receivers for short wireless links that use high carrier frequencies to avoid interference with the adjacent cells. The main advantage of this approach compared with a previously demonstrated system [8] is operation in the linear regime that can be more efficient and more stable.

Note that for nonlinear modulation the laser wavelength has to be locked to the minimum transmission point of the modulator. This is significantly more difficult to achieve compared with locking to the middle of the slope transfer function for the linear modulation case. Locking to a maximum or minimum of the transfer function (where the first derivative is zero) requires an advanced feedback mechanism [13]. Moreover the efficiency of small-signal linear modulation is typically larger than the efficiency of nonlinear modulation for both the MZ and microdisk device.

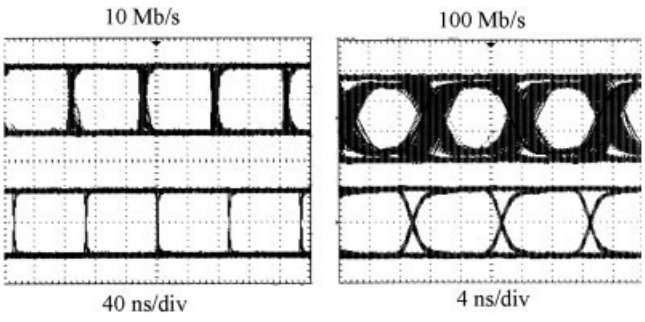

Figure 6 Measured eye diagrams of the detected down-converted NRZ PRBS data from a 14.6 GHz RF carrier using $LiNbO_3$ microdisk modulator [Fig. 5(b)] and FBG filter [Fig. 4(a)]

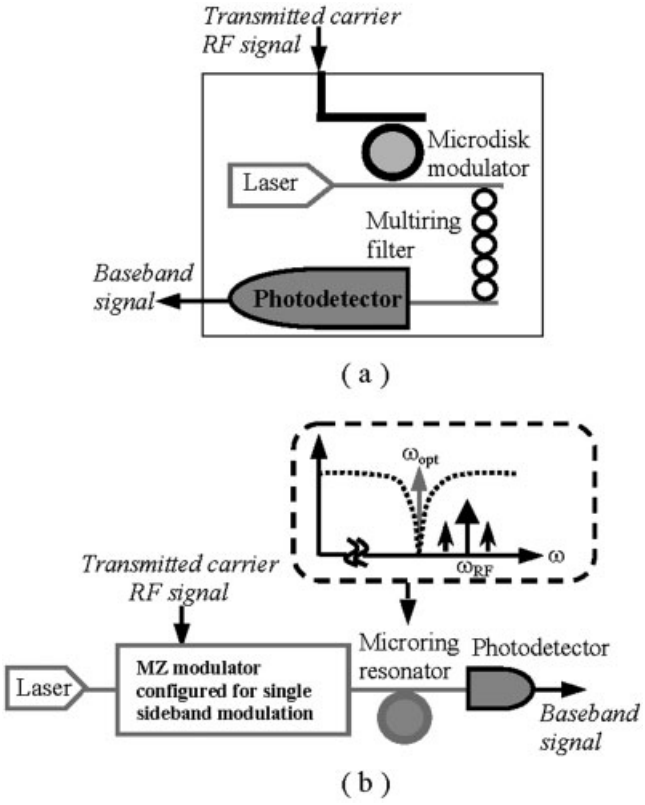

Figure 7 Schematic diagram of a photonic selfhomodyne RF down conversion system using (a) a band-pass multimicroring filter and (b) a microring notch filter

REFERENCES

1. R.A. Minasian, Photonic signal processing of microwave signals, IEEE Trans Microwave Theory Tech 54 (2006), 832–846.
2. W.S.C. Chang (Ed.), RF Technology in optical fiber links, Cambridge University Press, Cambridge, England 2002.
3. J. Lu, H. Chi, X. Zhang, and L. Shen, Noise reduction using photonic microwave filter for radio over fiber system, Microwave Opt Technol Lett 48 (2006), 305–307.
4. A. Hirata, M. Harada, and T. Nagatsuma, 120-GHz wireless link using photonic techniques for generation, modulation, and emission of millimeter-wave signals, J Light Wave Technol 21 (2003), 2145–2153.
5. K.-I. Kitayama and R.A. Griffin, Optical down-conversion from millimeter-wave to IF-band over 50-km-long optical fiber link using an

electroabsorption modulator, IEEE Photon Technol Lett 11 (1999), 287–289.
6. A.A. Abidi, Direct-conversion radio transceivers for digital communications, IEEE J Solid-State Circ 30 (1995), 1399–1410.
7. M. Tsuchiya and T. Hoshida, Nonlinear photodetection scheme and its system applications to fiber-optic millimeter-wave wireless downlinks, Microwave Theory Tech IEEE Trans 47 (1999), 1342–1350.
8. M. Hossein-Zadeh and A.F.J. Levi, 14.6 GHz $LiNbO_3$ microdisk photonic self-homodyne RF receiver, IEEE Microwave Theory Tech (special issue on Microwave Photonics) 54 (2006), 821–831.
9. M. Hossein-Zadeh and A.F.J. Levi, RF Mixing in $LiNbO_3$ microdisk modulator, IEEE/LEOS summer topical meetings 2004, MC4: WGM microcavities IV.
10. B.E. Little, S.T. Chu, P.P. Absil, J.V. Hryniewicz, F.G. Johnson, F. Seiferth, D. Gill, V. Van, O. King, and M. Trakalo, Very high-order microring resonator filters for WDM applications, IEEE Photon Technol Lett 16 (2004), 2263–2265.
11. A. Loayssa, C. Lim, A. Nirmalathas, and D. Benito, Simple optical single-sideband modulator for fiber-radio applications, Electron Lett 39 (2003), 97–99.
12. A.L. Campillo, Polarization-based single-sideband suppressed carrier modulator, IEEE Photon Technol Lett 18 (2006).
13. T. Carmon, T.J. Kippenberg, L. Yang, H. Rokhsari, S.M. Spillane, and K.J. Vahala, Feedback control of ultra-high-Q microcavities: Application to micro-Raman lasers and microparametric oscillators, Opt Express 13 (2005).

EFFICIENT FINITE ELEMENT ELECTROMAGNETIC MODELING OF THIN WIRES

Hong Wu and Andreas C. Cangellaris
Department of Electrical and Computer Engineering, University of Illinois at Urbana-Champaign, 1406 West Green St., Urbana, IL 61801; Corresponding author: cangella@uiuc.edu

Received 1 July 2007

ABSTRACT: *A computationally efficient methodology is presented for the finite element modeling of thin conducting wires of diameter comparable with or smaller than the numerical grid size. The proposed model relies upon the insertion of lumped circuit elements at element edges along the wire axis and the proper compensation of the electric permittivity and magnetic permeability values for mesh elements in the immediate neighborhood of the wire to reproduce the electromagnetic attributes of the wire accurately. In this manner, the need for local mesh refinement along the wire is eliminated. The proposed model is useful for the computationally efficient finite element modeling of inhomogeneous structures with wire antennas attached to them and of electronic packaging structures for high-speed integrated circuits containing wire bonds and high-density vertical interconnects.* © 2007 Wiley Periodicals, Inc. Microwave Opt Technol Lett 50: 350–354, 2008; Published online in Wiley InterScience (www.interscience.wiley.com). DOI 10.1002/mop.23060

Key words: *finite elements; thin wire modeling; signal integrity*

1. INTRODUCTION

Electronic packages for high-speed/high-frequency integrated circuits exhibit large variation in feature size, from micron-size for wire cross section to millimeter and centimeter for long wires. This multiscale attribute of electronic packages makes the direct application of finite element methods for their electromagnetic analysis cumbersome and computationally expensive. More specifically, the need to describe with good accuracy for the micron-size cross-sectional geometry of the wires makes mesh generation cumbersome. Furthermore, with grid size dictated in part by the micron-size features of the geometry, the finite element matrix becomes more ill-conditioned with undesirable effects on numerical solution robustness [1].

Wire antennas on platforms constitute another class of structures with similar challenges in the application of the finite element method for their electromagnetic analysis. In this article, a methodology is presented for containing the complexity of the finite element modeling of such structures. The proposed methodology extends the preliminary idea discussed in Ref. [2] of using lumped circuit elements at edges of the finite element mesh aligned along the wire axis to account for the internal impedance attributes of the wires.

With the wire cross-sectional dimensions assumed to be a very small fraction of the minimum wavelength of interest, and also much smaller than the wire length, the benefit resulting from "collapsing" the finite cross section of the wire to zero is clearly demonstrated through the example depicted in Figures 1(a) and 1(b). Shown in Figure 1(a) is the cross-sectional view of a finite element mesh used to model a thin wire. The mesh refinement in the immediate neighborhood of the wire, which is needed to resolve the wire cross section is apparent. Shown in Figure 1(b) is the cross-sectional view of the mesh that would be needed if the wire was assumed to be infinitesimally thin. As mentioned above, for such a case it is assumed that the finite element mesh is such that the wire axis runs along a set of cascaded edges of the mesh. In Figure 1(a), the number of nodes is 1168 nodes and the number of triangles 2239. In contrast, for the mesh in Figure 1(b) only 314 nodes and 561 triangles are used. This amounts to a three-fold reduction in the number of unknowns in the finite element model.

The approximation of the finite cross section wire by one which is infinitesimally thin must be complemented by appropriate modifications in the development of the finite element model to reinstate the electromagnetic properties of the wire, namely, its internal impedance and the correct field behavior in its immediate vicinity. The way this is done is presented in Section 2. In Section 3, the validity and accuracy of the proposed methodology are demonstrated through its application to an interconnect and a wire antenna structure.

2. PROPOSED METHODOLOGY

2.1. Wire Effective Radius

For the purposes of this discussion it is assumed that the wire is aligned along a cascaded set of edges of the finite element mesh. Furthermore, it is assumed that the mesh size (length of each edge) is a small fraction of the minimum wavelength of interest. To compensate for the approximation of a finite cross section wire by an infinitesimally thin one we must identify ways in which we can re-instate in the model the internal impedance of the wire and the proper field behavior in its immediate neighborhood. The former can be accomplished through the assignment of lumped circuit elements at the edges of the mesh along which the wire is aligned. This is discussed is the next subsection. With regards to the latter, its handling has to take into consideration the fact that the spatial sampling of the fields introduced by the finite element discretization makes the infinitesimally thin wire behave like a wire of a finite cross section. Thus, the first step in our development involves the computation of an effective cross-sectional dimension (effective radius) for the infinitesimally thin wire. The way in which this effective radius is computed in terms of the finite element mesh properties is discussed next.